Development of a Pneumatic Vibratory Wrist for Robotic Assembly

° Kyu Won Jeong* and Hyung Suck Cho**

* Ph.D Student
** Professor, Department of Production Engineering
Korea Advanced Institute of Science and Technology,
P.O.Box 150, Chongryangri, Seoul, Korea

Abstract

In this paper a pneumatic vibratory wrist with PWM controller is developed for robotic assembly. Since the vibration characteristics are critical to assembly performance, they are investigated both theoretically and experimentally. The results show that within a wide range of conditions the wrist vibration can be effectively used for precision assembly.

1. Introduction

It is more difficult that the robotic assembly system mates parts if the parts to be assembled become more precise, because many components of the assembly system cause position error. To cope with this problem many compliant devices such as RCC[1] device were developed. However, these devices can be applied to parts having chamfer which guide a male part into a female part at the early stage of insertion. On the other hand, vibratory assembly system can accomplish random search of a hole without intensive search algorithm. At the instance when the alignment is established, the insertion force pushes the male part into the hole. This method can be used for non-standard component assembly or mating chamferless parts. The vibratory assembly system have been developed by several investigators[2-8]. Most of the previous works of the vibratory assembly method have limitations in mating precise parts such as a fixed vibratory trajectories, furthermore, the characteristics of the devices have not been fully analyzed.

In this paper a vibratory assembly device is developed to enable the insertion task of precise parts, which can be fitted between the robot last joint and the end effector. The wrist is operated by pneumatic actuators in two direction (x and y) and its vibratory motions are induced via the pneumatic PWM controller which incorporates with a sensor signal. The output positions are measured by gap sensors and fedback to PI controllers. To analyze the characteristics of the wrist a mathematical model is derived, which represents the dynamics of the PWM-controlled system. Using the derived nonlinear model a series of simulations were performed to analyze the vibration amplitude and the vibratory trajectory of the wrist. These simulation results are verified by a series of experiments.

2. Description of the Pneumatic Vibratory Wrist

The major components of the pneumatic vibratory wrist are composed of a moving load, two cylinders, two solenoid valves and two flow control valves as shown in the Fig.1. The wrist motion occurs in two axis, e.g. x axis and y axis which are perpendicular to each other. The pneumatic system and the controller of the both axes have same construction. The position of the gripper loading unit is measured by a gap sensor and fedback to the PI controller. The PI controller output becomes the control input signal(u) to the Pulse Width Modulator. The modulator, then compares the control input with the carrier voltage and produces the solenoid valve driving signal. Fig.2 shows a block diagram of the position control system using PWM controller.

As shown in the figure, the pneumatic components are grouped into two parts which are discriminated by the subscript 1 or 2. A three-way directional solenoid valve is connected to each port of the cylinder and controls the air flow going into each cylinder. When a solenoid is energized (on-state), the inlet orifice is fully opened while the outlet orifice is closed at the same time. Then, the compressed air is fed to one chamber of the

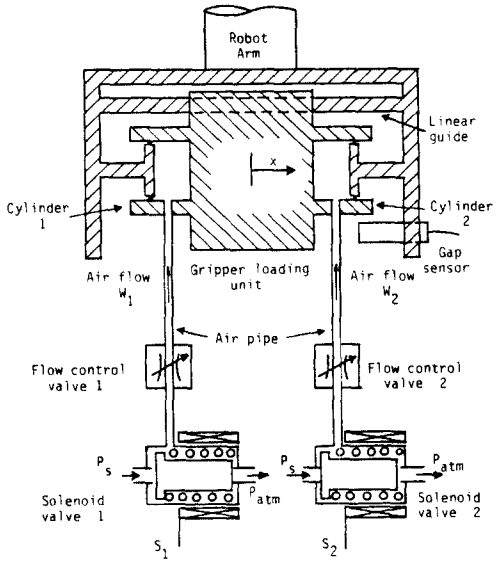

Fig.1 Schematic diagram of the wrist

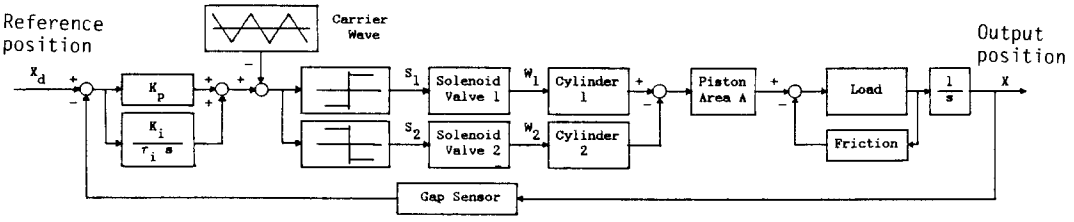

Fig.2 Block diagram of the control system for the vibratory wrist

cylinder through the inlet port of the valve. When the solenoid is de-energized (off-state), the inlet orifice is closed by the return spring, while the outlet orifice is fully opened. Then, the air in the chamber of the cylinder is exhausted through the outlet port of the valve. At any instance, as one solenoid valve is energized, the other solenoid is de-energized. When the solenoid valve 1 is energized, the solenoid valve 2 is de-energized. This causes the the cylinder 1 to move to the right to give a positive actuating force. However, the situation is reversed when the valve 2 is energized. In this case the flow into the cylinder occurs to give a negative actuating force. Therefore, the effective actuating force is obtained in the sense of time average. In the following sections the PWM controller and characteristics of the pneumatic system are analyzed. Although the mass and friction force of each axis are different from each other, only x axis is theoretically analyzed since both axes are found to have same trends in vibration characteristics.

2.1 Vibration Control System

PI controller

In this vibratory wrist a PI controller is used to obtain accurate position. The position of the gripper loading unit is measured by a gap sensor, to obtain accurate position. The position of the gripper loading unit is measured by a gap sensor, and then fedback to the PI controller, as shown in Fig.2. If x_d and x denotes the reference position and the actual position from center position, respectively, then the control input is given by

$$u = K_p K_s (x_d - x) + \frac{K_i}{\tau_i} \int_o^t K_s (x_d - x) d\tau \qquad (1)$$

In the above K_p is the proportional gain, K_s is the gap sensor gain, K_i is the integral gain and τ_i is the integral time constant.

Pulse Width Modulator

Pneumatic control systems utilizing PWM were constructed by several investigators[9,10,11]. They considered the PWM as a constant gain, and did not analyze the vibratory characteristics. A solenoid driving signal according to the input u is shown in Fig.3. The carrier wave E(t) is symmetrical triangular form and can be expressed by Ref.[9].

$$E(t) = \begin{cases} E_m/(T_c/4)h & \text{for } 0 \leqq h < T_c/4 \\ -E_m/(T_c/4)(h-T_c/4)+E_m & \text{for } T_c/4 \leqq h < 3T_c/4 \\ E_m/(T_c/4)(h-3T_c/4)-E_m & \text{for } 3T_c/4 \leqq h < T_c \end{cases} \qquad (2)$$

where,

$h = t - nT_c$ (n=0,1,2 ...)

E_m : magnitude of carrier wave (voltage)

T_c : period of carrier wave (sec)

Comparing u of eq.(1) with E(t) of eq.(2), the modulator generates a series of width modulated pulses S_1 and S_2 as shown in Fig.3.(b) and (c) as follows.

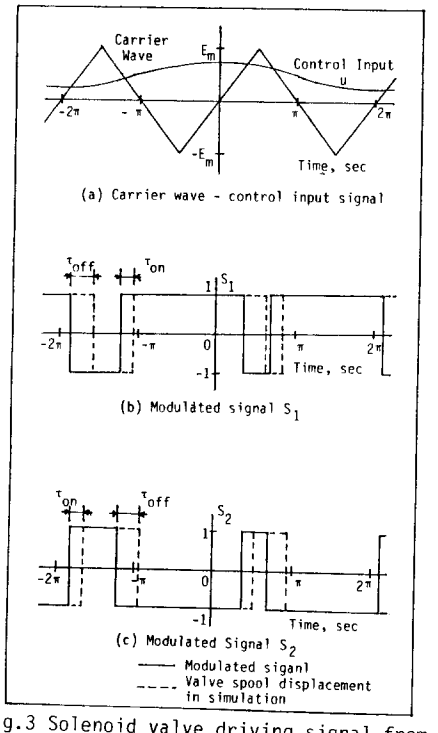

Fig.3 Solenoid valve driving signal from Pulse Width Modulator

$$S_1(t) = \begin{cases} 1 & u(t) \geq E(t) \\ -1 & u(t) < E(t) \end{cases} \qquad (3)$$

$$S_2(t) = -S_1(t)$$

The modulated signal S_1 is analyzed in detail to investigate the influence of the PWM on the vibration characteristics. In general, the modulator input signal u given in eq.(1) is composed of D.C. component $\bar{u}$ and A.C. component u_a which has an angular velocity ω'. Then, u is described by

$$u = \bar{u} + u_a \cos(\omega' t), \qquad (4)$$

For this control input, the PWM output pulse train S_1 or S_2 can be expressed by a double Fourier series[12]. The magnitude of the higher order terms are relatively small as compared with the other terms and the solenoid valve can not be operated in such a high frequency. Therefore, the width modulated pulse train(S_1 or S_2) could be approximated up to the first order as follows:

$$S_1(\bar{u}, u_a, t) = \frac{\bar{u}}{E_m} + \frac{4}{\pi} J_o\left(\frac{\pi u_a}{2 E_m}\right) \cos\left(\frac{\pi \bar{u}}{2 E_m}\right) \sin(\omega t). \qquad (5)$$

where J_o is the zero-order Bessel function. and ω is the angular velocity of the carrier wave. The modulated signal S_2 is given in eq.(3).

$$S_2(\bar{u}, u_a, t) = -S_1(\bar{u}, u_a, t) \qquad (6)$$

The solenoid driving signal S_1(or S_2) consists of two parts, the first part is a D.C. component whose magnitude is $\bar{u}/E_m$ and the second parts is a sinusoidal harmonic term. If the sinusoidal harmonic term can be negligible, the PWM controller can be considered as a constant gain of $1/E_m$. From eq.(2), we can find that when u has only maximum D.C. component i.e. $u=E_m$, the S_1 and S_2 value become $S_1=1$ and $S_2=-1$. This means that solenoid valve 1 is continuously energized and pressurizes air to flow into the cylinder 1, while solenoid valve 2 is continuously deenergized and air flow occurs from the cylinder 2 to the atmosphere. On the other hand, when u=0, the actuating input of the system becomes zero in the system using a linear servo valve. However, in the case utilizing PWM method, S_1 becomes $S_1=(4/\pi)\sin(\omega t)$. As a result the position output of the wrist is oscillated with same frequency as the carrier wave. These characteristics could be effectively used in the robotic assembly task.

2.2 Dynamic Model of the System

The pneumatic process of the charging or discharging process and the flow rate through an orifice were analyzed in ref.[13,14,15]. The processes are assumed to be adiabatic as in the case of fast acting process and furthermore, reversible process.

$$\dot{P}_1 = -\frac{kA\dot{x}}{V_o + Ax} P_1 + \frac{k\,Ts_1\,R}{g} \frac{W_1}{V_o + Ax} \qquad (7)$$

$$\dot{P}_2 = \frac{kA\dot{x}}{V_o - Ax} P_2 + \frac{k\,Ts_2\,R}{g} \frac{W_2}{V_o - Ax}$$

In the above $\dot{}$ denotes time derivative and the subscripts 1 and 2 represent both side of the cylinder as shown in the Fig.1. W denotes the weight flow rate to the chamber V. Ts denotes the stagnation temperature. P represents the chamber pressure, R is the gas constant of the air, g is the gravity acceleration, k denotes the specific heat ratio of the air, A is the cross section area of the cylinder and V_o is the volume of the chamber at steady state.

The weight flow rate of the air through a single orifice is given by[13].

$$W = W(A_e, P_u, P_d, Ts_u)$$

$$= 1.532\, A_e \frac{P_u}{\sqrt{Ts_u}} \left(\frac{P_d}{P_u}\right)^{\frac{1}{k}} \sqrt{1 - \left(\frac{P_d}{P_u}\right)^{\frac{k-1}{k}}} \quad \text{for } \frac{P_d}{P_u} \geq 0.528$$

$$= 0.3965\, A_e \frac{P_u}{\sqrt{Ts_u}} \quad \text{for } \frac{P_d}{P_u} < 0.528 \qquad (8)$$

where P_u and P_d represent the upstream pressure and downstream pressure, respectively, A_e is the effective orifice area which is the orifice area multiplied by the discharge coefficient, and Ts_u is the stagnation temperature of the upstream.

For the mechanical part consisting of the gripper loading unit, the dynamic equation of the system is given by

$$A(P_1 - P_2) = \frac{M_x}{g} \ddot{x} + B\dot{x} + Fr - F\ell \qquad (9)$$

where M_x is the mass of the gripper, $\dot{x}$ and $\ddot{x}$ denote the velocity and acceleration of the mass, respectively, B denotes the viscous friction coefficient, Fr is the coulomb plus stiction friction force, and the $F\ell$ denotes the external load.

Solenoid Valve Model

Although the solenoid valve is energized by the solenoid current according to eq.(2), because of the dynamics of the solenoid and the spool and return spring system, there is always a time delay between valve driving signal change and actual opening of the orifice. When the solenoid valve is opened, the spool is actuated by the electromagnetic force of the solenoid and by the high pressure air supply. On the other hand, when the solenoid valve is closed, the spool is actuated only by the return spring against the high pressure air supply. Therefore, when the solenoid is opened, the time delay is shorter

than when it is closed. The solenoid valve dynamics are assumed to be pure time delaies as shown in the Fig.3(b) and (c). The delay time was obtained from the preliminary experiments.

3. Simulation and Experiment

Based upon the previous analysis, a series of the computer simulations and experiments were conducted (1) to obtain the amplitude characteristics of the vibration, and (2) to obtain the variation of vibratory trajectory with the carrier frequency.

Simulation Procedure

The simulation studies were performed using the previously obtained parameters. Using the nonlinear dynamic equations (1)-(3), (7)-(9) and the solenoid valve dynamics, a series of simulations were performed via a 4th order Runge-Kutta method with integration time 0.2msec. The system parameters used in the simulations and experiments are shown in Table 1. The atmosphere pressure is assumed to be 1 kgf/cm^2 and the stagnation temperature of the air is assumed as $298.15^{o}K$. The parameters, such as specific heat ratio k and the stagnation temperature Ts, are dependent on the air condition, but the nominal values k=1.4 and $Ts=298.15^{o}K$ were used in the simulation. The piston area(A) and the cylinder volume including the air pipe volume(V_o) were determined from the manufacturer's data. The friction was modeled as in Fig.4 and the parameters related to the friction force were obtained to minimize the error between the experimental results and the simulation ones.

Experimental Procedure

Fig.5 shows the experimental setup which is composed of a wrist, a function generator which generates a triangular carrier wave, a Lab-Master (model TM-40 PGH) which contains D/A, A/D converters and counters, and a micro-computer (model IBM-XT). The position reference was generated via D/A converters of the micro-computer. The pneumatic circuit of the wrist is composed of many components; the cylinders (model ADV-12-10), the solenoid valves (model BMSFG-2-3-M5) and the flow control valves (model GRO-M5), all of which are made by FESTO Inc. The supply pressure P_s was regulated by an

Table 1 System parameters

P_s	6 Kgf/cm^2
P_{atm}	1 Kgf/cm^2
Ts	$298.15^{o}K$
A	1.131 cm^2
V_o	1.806 cm^3
E_m	$\pm$ 10 V
τ_{on}	0.005 sec
τ_{off}	0.01 sec
B_x	0.075 Kgf/(cm/sec)
B_y	0.085 Kgf/(cm/sec)

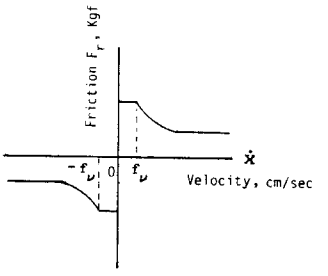

$$|F_r| = \begin{cases} F_{coul} + F_{stic} & \text{for } |\dot{x}| \le f_\nu \\ F_{coul} + F_{stic}\,EXP[-f_s(|\dot{x}|-f_\nu)] & \text{for } |\dot{x}| > f_\nu \end{cases}$$

Axis	Mass (Kg)	F_{coul} (Kgf)	F_{stic} (Kgf)	f_s (sec/cm)	f_ν (cm/sec)
X	2.15 3.15	0.37 0.42	0.27 0.34	3.5 3.5	0.54 0.54
Y	1.7	0.79	0.42	3.5	0.54

Fig.4 Friction model in computer simulation

air regulator as P_s=6 Kgf/cm^2. The actual position was measured by an inductive type gap sensor(Ono-Sokky) and acquired by the micro-computer through the A/D converters. The sampling time was fixed at 3msec for all experiments.

4. Results and Discussions

Vibratory magnitude

The wrist is oscillated with the carrier frequency as explained previously. The magnitude of the vibration is dependent on the system parameters as shown in the mathematical modelling of the system. Throughout the experiments the carrier frequency, the orifice area of the flow control valve, and the masses were varied to investigate the effect of these parameters on the vibration characteristics. The effective orifice areas were varied as $2.666x10^{-4}cm^2$, $3.635x10^{-4}cm^2$, and $5.089x10^{-4}cm^2$. The masses were

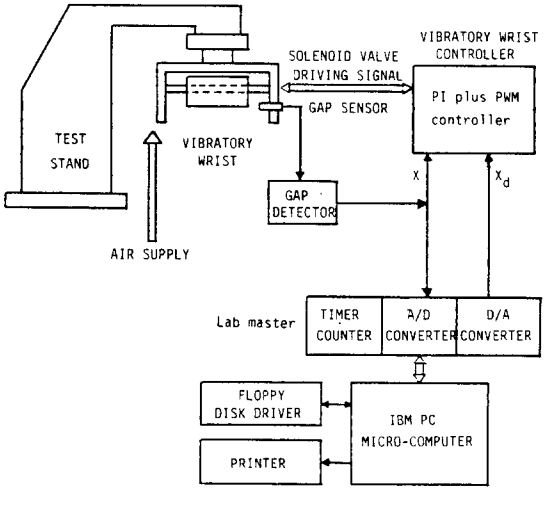

Fig.5 Schematic diagram of the experimental setup

2.15Kg and 3.15Kg. The other parameters and reference position were kept the same as those used in the previous experiments. Ten experiments were performed at each orifice area and carrier frequency. The experimental results and simulation results of the magnitude of vibration are shown in Fig.6. It can be seen that the magnitude is decreased as the carrier frequency is increased. At high carrier frequency the magnitude is drastically decreased, because the air has relatively larger fluid compliance than the hydraulic oil and there are friction at the cylinder and time delay of the solenoid valve. The magnitude is also increased as the orifice area is increased. On the other hand, from the Fig.6.(a) and (b) it can be also found that the magnitude is decreased when the mass is increased.

Vibratory trajectory

To examine the vibratory trajectory of the wrist, both x axis and y axis were simultaneously operated. The effective orifice areas of x axis and y axis were fixed at $5.089 \times 10^{-4} cm^2$ and $8.461 \times 10^{-4} cm^2$, while the masses were 2.15Kg and 1.7Kg, respectively. Since the wrist motion is much dependent on the difference between the carrier frequencies of both axes, the experiment and simulation were conducted in the manner both axes have different carrier frequencies from each other, They were selected typically as f_x=14Hz and f_y=16Hz in Fig.7. The time responses are shown in Fig.7.1.(a) and (b). In the figure it can be also found that the vibration frequency is same as the carrier frequency as shown in eq.(5). The covering area in the phase plane is determined by the vibration magnitude of the both axes as shown in Fig.7.1.(c). A little difference is observed between the experimental result in Fig.7.2 and the simulation ones in Fig.7.1 due to the un-modeled dynamics e.g. that of the air supply. With such vibration mode the wrist can perform the search motion within the region as shown in the figure.

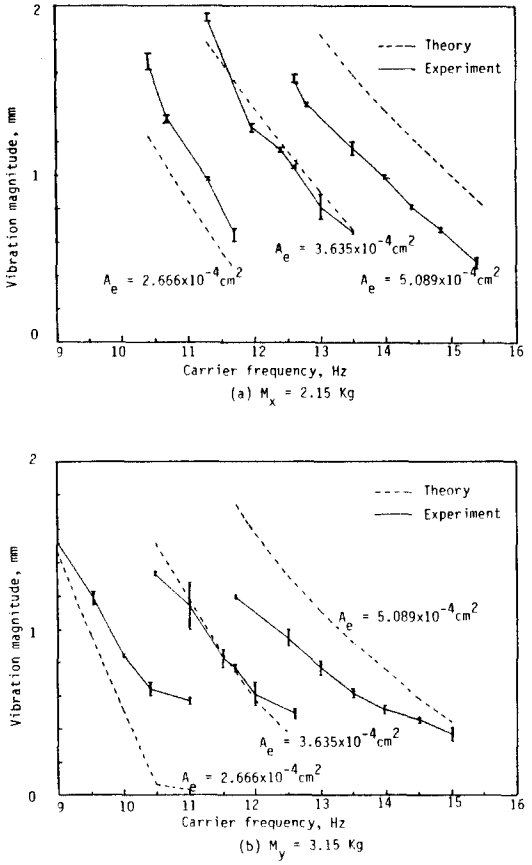

Fig.6 Vibration magnitude with carrier frequency
System parameters: K_p=1.54, k_i=0, τ_i=0.25sec

5. Concluding Remarks

A mathematical model of the PWM controlled vibratory wrist has been derived in order to investigate its vibration characteristics. Based upon the derived mathematical model, the characteristics of the vibration were clarified by a series of simulation. The results of this theoretical analysis were verified by experiments. Both results are relatively in good agreement.

Based upon the results obtained in the experiments and computer simulations, the following major conclusions can be made:(1) The magnitude of the vibration can be controlled by the carrier frequency and the orifice area of the flow control valve. The vibration magnitude can be increased by decreasing the carrier frequency or by increasing the orifice area of the flow control valve. Also it is increased when the mass is decreased. (2) The phase plane trajectory can be controlled by varing the carrier frequency. The wrist is able to cover large area when the carrier frequencies of the both axes are different each other. These results indicate the vibration mode induced by the wrist can be effectively used at the search stage for part mating.

References

[1] D.E.Whitney, "Quasi-static assembly of compliantly supported rigid parts", J. Dynam. Systems, Measur. Control. 104,March, 1982, pp.65-77

[2] V.M.Savishchenko and V.G.Bespalov, "The orientation of components for automatic assembly", Russian Engineering Journal, 45, No.5, 1965, pp.50-52

[3] N.M.Karelin and A.M.Girel, "The accurate alignment of parts for automatic assembly", Russian Engineering journal Vol.47,No.9, 1967, pp.73-76

[4] G.Ya.Andreev, et. al., "Assembly joints by magnetic method of orientation", Russian Engineering Journal, 56, No.4, 1976 pp.68-71

[5] A.M.Girel, "Using a rotation magnetic field for the grippers of industrial robots", Russian Engineering Journal, 57, No.6, 1977, pp.43-45

[6] Unimation Inc.,"Programmed manipulator apparatus for assembly parts", UK patent spec.1437003, May 1976

[7] B.D.Hoffman,S.H.Pollack and B.Weissman, "Vibratory Insertion Process: A new approach to nonstandard component insertion", Robot 8,July 31, 1985 pp.8-1-8-10

[8] H.J.Warnecke, B. Frankenhauser, D.G.Gweon and H.S.Cho, "Fitting of crimp contacts to connectors using industrial robots supported by vibrating tools", submitted to Robotica

[9] S.G.Lee and H.S.Cho, "On the development of a PWM control based pneumatic servomechanism", Int. Sysmp. on Fluid Control and Measurement, Tokyo, Sept. 2-6 1985, pp.37-46
[10] Y.Morita, M.Shimizu, and T. Kagawa, "An analysis of pneumatic PWM and its application to a manipulator", Int. Sysmp. on Fluid Control and Measurement, Tokyo, Sept.2-6 1985, pp.3-8
[11] T.Noritsugu, "Pulse-Width-Modulated feedback force control of a pneumatically powered robot hand", Int. Sysmp. on Fluid Control and Measurement, Tokyo, Sept.2-6, 1985, pp.47-52
[12] H.S.Black, Modulation Theory, Van. Nostrand Reinhold Co., 1953, pp.263-280
[13] C.R.Burrows, Fluid power servomechanisms, Van Nostrand Reinhold Co. London 1972
[14] B.W.Andersen, The analysis and design of pneumatic systems, John Wiley & Sons,Inc., 1967
[15] J.L.Shearer, "Study of pneumatic process in the continuous control of motion with compressed air I,II", Trans. of the ASME, 78, No.2, Feb. 1956 pp.233-249

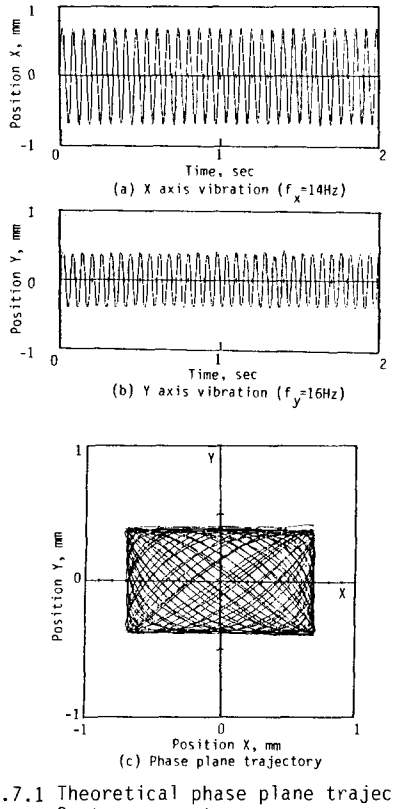

Fig.7.1 Theoretical phase plane trajectory
System parameters:

M_x=2.15Kg, f_x=14Hz, A_{ex}=5.089x10^{-4}cm^2
M_y=1.7 Kg, f_y=16Hz, A_{ey}=8.461x10^{-4}cm^2

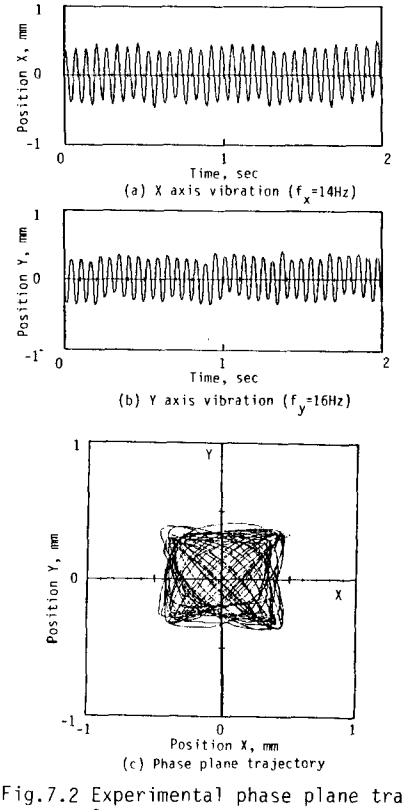

Fig.7.2 Experimental phase plane trajectory
System parameters:

M_x=2.15Kg, f_x=14Hz, A_{ex}=5.089x10^{-4}cm^2
M_y=1.7 Kg, f_y=16Hz, A_{ey}=8.461x10^{-4}cm^2